J Mater Sci (2007) 42:7116–7122
DOI 10.1007/s10853-007-1550-9

Reactionary processes during mechanical treatment of mixtures of ZnO and MnO_2. I. Formation of defects and solid solution

Mykola Kakazey · Marina Vlasova · Martha Dominguez-Patiño · Ismael Leon · Momcilo Ristic

Received: 30 October 2006 / Accepted: 24 January 2007 / Published online: 5 May 2007

Abstract Kinetics of defects formation, reaction process and formation of solid solution in powder mixtures of ZnO and MnO_2 induced by prolonged mechanical treatment (MT) have been investigated (X-ray, FTIR, EPR). At MT in zones of deformation-destruction the different defects (V_{Zn}^{-} : Zn_i^0 (**I**), V_{Zn}^{-} (**II**), and $(V_{Zn}^{-})_2^{-}$ (**III**) centers at all) are forming. The defects have various physical and chemical properties, and have different activation energies of annealing, E_{act} The part of these defects is responsible for the processes of hydration and carbonation of samples. In turn, the formation of defects is accompanied by development of various mechanothermical processes, which increase temperature of the sample, T_{MT}, with the increasing of duration of MT, t_{MT}. The increasing of t_{MT} activates the reactionary processes: promotes a consecutive annealing the «low-temperature» defects having small values of E_{act} (**I**, **II** and **III**) and also leads to formation of Mn^{2+}-doped $Zn(OH)_2$. With the further increase of $t_{MT,}$ the process of MT is accompanied by an increasing of temperature of samples up to equilibrium, T_{eq} and accumulation of ''high-temperature'' defects in the sample. As a result, in the sample the conditions for intensification of volumetric diffusion processes and formation of Mn^{2+}-doped ZnO were created.

M. Kakazey (✉) · M. Vlasova · M. Dominguez-Patiño
CIICAp-Universidad Autonoma del Estado de Morelos, Cuernavaca, Mexico
e-mail: kakazey@hotmail.com

I. Leon
CIQ-Universidad Autonoma del Estado de Morelos, Cuernavaca, Mexico

M. Ristic
Serbian Academy of Sciences and Arts, Belgrade, Serbia

Introduction

The doping of ZnO by various impurities, in order to modify its electro conductivity, is used in formation of nonlinear properties of varistor ceramics [1]. In the last years interest in doping ZnO + transition group oxide systems has increased in connection with the development of diluted magnetic semiconductors [2]. A number of studies have shown a marked solubility of Mn atoms in ZnO using various doping methods (e.g., the use of hydrothermal techniques) [3]. Thin $Zn_{1-x}Mn_xO$ films have been prepared by: pulsed-laser deposition [4–6], laser molecular-beam epitaxy [7, 8], sol-gel method [9], hydrolysis and condensation reaction [10], RF magnetron sputtering [11], and solid state reaction at different temperatures [12–14]. It has been shown that the solubility of Mn in ZnO at 600 °C is 12% and at 800 °C is 25% [3]. In another study [5, 6], the solubility of Mn in the ZnO matrix was increased ($x \leq 35\%$), and these samples showed high temperature ferromagnetism [5, 6]. However, it has been shown [14, 15] that the solubility limit for Mn in the ZnO matrix is ~10%, and that the high temperature ferromagnetism [5, 6] is attributable to second phase formation. Moreover note that in 1966 it was shown that Mn solubility in ZnO is low, less than 2 mol% in the 600–1,450 °C temperature range [16].

In this study, we report formation of a solid solution of ions Mn^{2+} in ZnO lattice by a method of mechanical treatment (MT) of mixtures of ZnO and MnO_2. This study provides information about the production and behavior of native defects in ZnO with increasing time. Defects in zones of destruction are subjected to: the local hyper-rapid ultrahigh-temperature spike (in moment of destruction), the significantly prolonged collective high-temperature influences (in moment of loading by balls), and accumulative

thermal effects. The increase of concentration of defects in ZnO, temperature of the sample with the increasing of MT duration, t_{MT}, creates favorable preconditions for ''mechanical'' doping of ZnO by ions of manganese.

Experiments

The starting materials were commercially available ZnO (>99% purity, Reasol, Milan, Italy; Corresponds to the specification of the American Chemical Society) and MnO_2 (99.26% purity; J. T. Baker; Mexico). Electron microscope studies (Scanning electron microscopy, model LEO 1450 VP, LEO Electron Microscopy Inc., Thornwood, NY) showed that the average size of particle was $d_{ZnO} \approx 0.25$ μm and $d_{Mn2O3} \approx 0.3$ μm. Mixtures of powders with two different compositions, i.e., ZnO + 1 wt.% MnO_2 (sample ***a***) and ZnO + 10 wt.% MnO_2 (sample ***b***), were investigated.

MT of samples was carried out in Planetary Ball-Mill (type PM 400/2, Retsch Inc.). Grinding jars of two types were used: (1) jars of volume 250 ml and balls (10 of 20 mm, 15 of 12 mm, and 25 of 10 mm) from stainless steel; (2) jars of ''comfort'' (volume 50 ml) and balls (3 of 20 mm and 10 of 10 mm) from tungsten carbide. The ratio of the balls to powders was ~7:1 in weight. The MT was carried out in air (in hermetically sealed jars) with a maximal (for this mill) rotation rate of 400 rev min^{-1}. It was established that MT in jars of 250 ml (from stainless steel) introduces in the samples small magnetic iron particles. As the presence of such type of particles led to distortion of EPR, SEM and IR-results, the maximal duration of MT in these jars was limited to 1 h. According to the results of quantitative spectral analysis the content of contamination of iron in such sample was about 0.2%.

Duration of the milling, t_{MT}, of powders in jars from tungsten carbide (50 ml) was: 1, 3, 6, 30, 90, 390, 750, 2,190, and 2,880 min. Note that the content of contamination of tungsten in the samples processed in 50 ml the jar during 2,880 min did not exceed 0.02%. In the work we made supposition that such amount of the contamination do not influence on observed changes.

X-ray difractometer (Siemens D-500, Siemens (now Bruker AXS) Karlsruhe, Germany) with Cu$K\alpha$ radiation was used for phase identification of the milled powder mixtures and determination of the average size of crystallites, D, and microstress, ***e*** (Δa/a). The average size of crystallites was determined using the Scherrer formula [17]:

$$B_p(2\theta) = 0.9\lambda/D\cos\theta, \quad (1)$$

where $B_p(2\theta)$ is the line broadening (in radians) due to the effect of small crystallites; λ is the wave length of the X-ray radiation and θ is the Bragg angle. The broadening in a peak due to microstress to be related to the residual strain ***e*** by

$$B_\varepsilon(2\theta) = 4e\mathrm{tg}\theta. \quad (2)$$

For interference Gaussian lines

$$B_h^2(2\theta) = B_p^2(2\theta) + B_f^2 + B_\varepsilon^2(2\theta), \quad (3)$$

where $B_h(2\theta)$ is the breadth of observed diffraction line at its half-intensity maximum, and B_f is an instrumental broadening (~0.003 rad). The experimentally observed broadening of several peaks can be used to compute the average size of crystalline D and the strain ***e*** simultaneously in ZnO samples.

Infrared (IR) spectrophotometer (Bruker Vector 22 FTIR, Karlsruhe, Germany, with resolution 4 cm^{-1}), in transmission mode was used for the present work. The samples were mixed with KBr in the ratio 2:60 and the resulting mixtures were pressed until obtaining transparent plates.

Electron Paramagnetic Resonance (EPR, SE/X 2547—Radiopan, Poznan, Poland) at room temperature were used for investigation of the formation different paramagnetic centres during MT of the ZnO + $x$$MnO_2$ powder mixtures.

Experimental results

The general supervision

Only on initial stage of MT (t_{MT} ~ 3 min, jars of volume 50 ml) the particles of powder were not aggregated noticeably and did not stick on walls of a jars and a surface of balls. With the increasing of t_{MT} the adhering of powder on walls of jars was observed. And the adhering was non-uniform. The bigger amount of the sample was localized in the bottom part of jars. It indicated on existence in jars of a zone with minimal crushing ability. Apparently, presence of such zone is defined by a design of a mill, jars, a set and the sizes of the balls, a treatment material. And balls are rolling along the layer of powder.

X-ray

XRD patterns of ***a*** and ***b*** samples as a function of the milling time are shown in Fig. 1. It can be seen that the initial ZnO and MnO_2 powders comprises primarily the

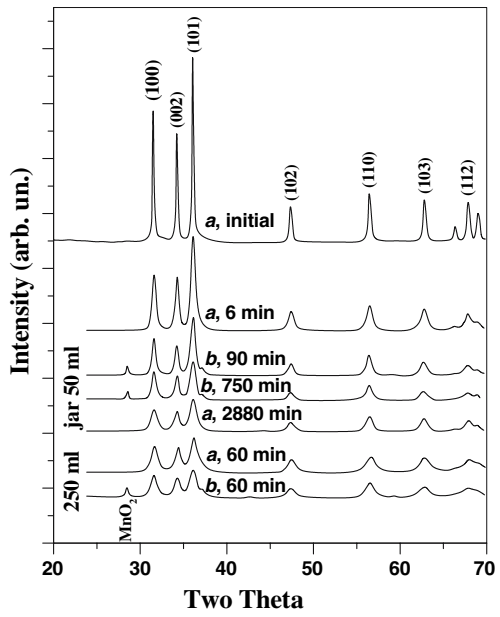

Fig. 1 X-ray diffraction patterns of samples ***a*** and ***b*** after MT during different t_{MT}

zincite and the pyrolusite polymorphs, correspondingly. Diffraction lines of ZnO and MnO_2 (β-MnO_2 tetragonal, line (110)) are broadening with the increasing of t_{MT}. This caused by the decreasing of crystallites sizes, D, and with appearance of internal strain, ***e***. On the based of the broadening of (100) and (103) peaks (Fig. 1) the size of crystalline and microstress in ZnO was calculated (see (3)). The value of D in initial ZnO is size of order of 180 nanometers. With the increasing of t_{MT} value of D is decreasing and value of ***e*** is increasing (Fig. 2, curves 1 (for ***b*** in jar of 250 ml) and curves 2 (for ***b*** in jar of 50 ml)). Values D and ***e*** in the samples grinded in a jar of volume of 250 ml for 60 min are approximately the same as in samples treated in a jar of volume of 50 ml for 2,880 min

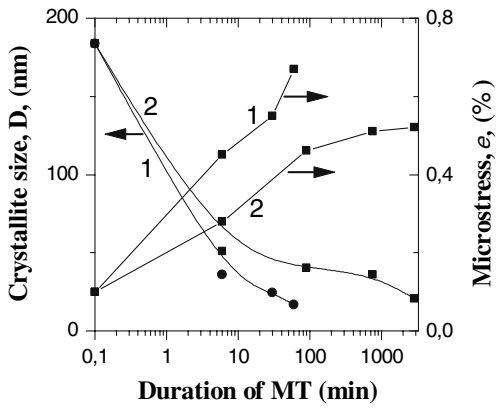

Fig. 2 Kinetics of the crystallites sizes, D, and microstress, ***e***, changes in ZnO (samples ***b***) during MT. 1—MT in jar of 250 ml; 2—MT in jar of 50 ml

(Fig. 2). This result showed that intensity of crushing-activation at MT in a jar of volume of 250 ml is considerably higher than processing in a jar of volume of 50 ml.

The area under of the zincite reflections was constant. But the area under diffraction (110) line of the MnO_2 (sample ***b***) decreases with the increasing of t_{MT}. This may be due to the phase transformation of β-MnO_2 tetragonal to other crystalline structures (MnO_2 orthorhombic, Mn_2O_3 at al.), or dissolution of MnO_2 and ZnO, or formation of the new phase product in system Zn–Mn–O. We did not observe formation of X-ray peaks of new phase products.

Infrared spectroscopy

The obtained FTIR spectra are given in Fig. 3. The careful analysis of spectra on Fig. 3 reveals several interesting features:

(a) there are two strong absorption peaks in initial sample: the ZnO stretching mode at ~450 cm^{-1} and peak at 3,500–3,300 cm^{-1} attributed to hydroxyl groups (adsorption of H_2O and formation of $Zn(OH)_2$). Weak peaks at $\nu \sim 2{,}925$ and 1,630 cm^{-1} belong to the vibrations of $–CH_2$ and C=O groups, respectively [18].

(b) With the increasing of t_{MT} (0–2,880 min) in sample ***a*** the gradual increasing of intensity of peaks at 3,500–3,300 cm^{-1}, 2,925 and 1,630 cm^{-1}, and formation and the increasing of peaks at $\nu \sim 1{,}480$–1,390 cm^{-1} ($–CO_3$ groups ($ZnCO_3$)), 1,000–700 cm^{-1} (C–C–O groups) is observed (see Figs. 3, 4); in sample ***b*** these transformations take place only at initial stages of MT ($t_{MT} \sim 0 \div 90$ min). As shown in Fig. 4, the intensity of the peaks decreases with the further increasing of t_{MT}:10 ÷ 2,880 min for adsorption of $–CO_3$ groups and 90–2,880 min for adsorption of H_2O. Note that curves in Fig. 4 reflect processes of quantitative changes of number of the defects responsible for hydration and carbonation (let's designate them as **H** and **C** defects) of a surface of MT particles ZnO.

Electron paramagnetic resonance

Figure 5 shows the EPR spectra of samples ***a*** and ***b*** after MT, taken at room temperature. Fig. 5 (a2, b2) shows the evolution of EPR spectra of electron-hole paramagnetic centers (PC) [19, 20] induced in ZnO at beginning stage of MT. Signal **I** is from the V_{Zn}^{-}:Zn_i^0 center with $g_\perp = 2.0190$, $g_{\|} < g_\perp$ [21]. Signal **II** is from V_{Zn}^{-} center with $g_\perp = 2.0130$, $g_{\|} = 2.0140$ [22]. Signal **III** is from $(V_{Zn}^{-})_2^{-}$ center with $g_1 = 2.0075$, $g_2 = 2.0060$, $g_3 = 2.0015$ [21]. These centers are formed in a zone of destruction. From the analysis of width of signals **I** ($\Delta B_I \approx 2.5$ Gs), **II** ($\Delta B_{II} \approx 3.0$ Gs) and

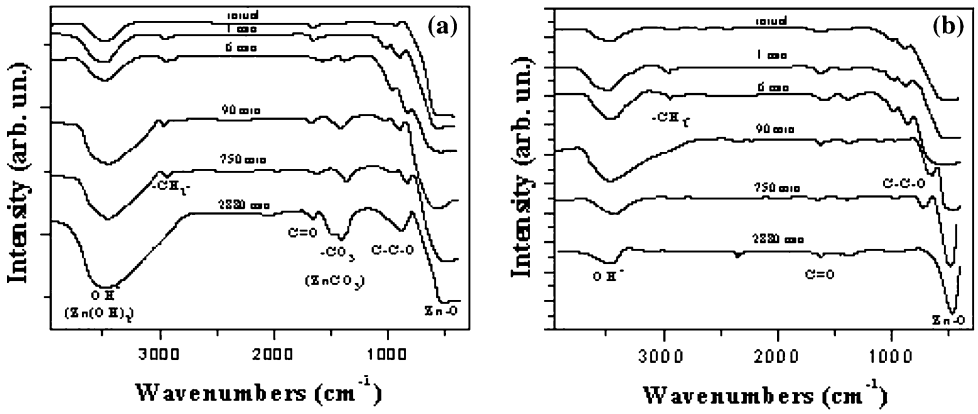

Fig. 3 FTIR transmission spectra of samples (***a***) (ZnO + 1%MnO2), and (***b***) (ZnO + 10%MnO2) depending on duration of mechanical treatment

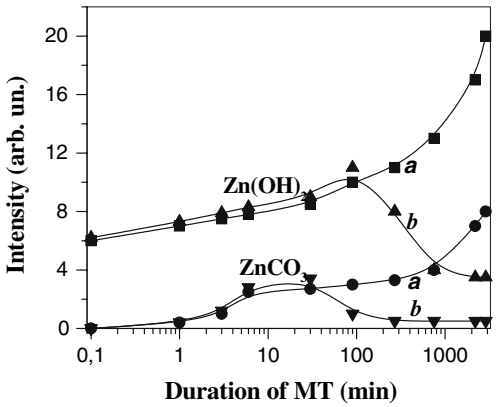

Fig. 4 The changes of intensities of peak at 3,500–3,300 cm^{-1} ($Zn(OH)_2$) (1, 2) and peaks at 1,480–1,390 cm^{-1} (–CO3 groups (ZnCO3)) (3, 4) for samples ***a*** (1, 3) and ***b*** (2, 4) as a function of duration of mechanical treatment

III ($\Delta B_{III} \approx 2.7$ Gs) it is possible to estimate that local concentration of **I**, **II** and **III** centers does not exceed 0.1 at.%. Note that unlike EPR-data for samples of pure ZnO [19], in these the formation of the V_O^+-centers (F^+-centre) and small donor centers (SDC) was not observed.

Starting with $t_{MT} = 90$ min in samples appears the sextet of lines, which belongs to signal **IV.** And starting with $t_{MT} = 390$ min in the samples is detected the sextet of signal **V** (see Fig. 5a1 and b1). Both spectra are connected with paramagnetic Mn^{2+}-centers. Similar spectra (S_I and S_{II}, accordingly) were observed in ZnO nanocrystals, prepared by reaction of Zn^{2+} and OH^- in solution of alcohol, with different surface conditions, modified by an annealing process [23]. In the work [23] spectrum S_I was attributed to isolated substitution Mn^{2+} ions in ZnO lattice. The second spectrum S_{II} was attributed to Mn^{2+} ions in $Zn(OH)_2$ lattice, which is present as a surface shell of the ZnO nanoparticles. However such interpretation of these spectra is incorrect.

EPR spectrum of Mn^{2+} ions in ZnO lattice is described by the rhombic spin-Hamiltonian

$$H = g\beta HS + 1/6a(S_x^4 + S_y^4 + S_z^4) + D[S_z^2 - 1/3\ S(S+1)] + ASI, \quad (4)$$

where S = 5/2 and all symbols have their usual meaning. In crystal $g = 2.0012$, $A = -76\cdot10^{-4}$ cm^{-1}, $D = 236\cdot10^{-4}$ cm^{-1} and $a = 6.2\cdot10^{-4}$ cm^{-1} [24]. Simulated [25] EPR spectrum Mn^{2+} ions in the polycrystalline sample of ZnO (the contribution of a member with parameter a was neglected) is presented in Fig. 5a1 (curve Mn^{2+}:ZnO). It is easy to see that the simulated spectrum corresponds to an experimental spectrum **V**. Hence, the spectrum **V** (S_{II} in [23]) belongs to isolated substitution Mn^{2+} ions in ZnO lattice. In Fig. 5a1 and b1 the calculated position of the central transitions singularities [26] is shown below the spectrum. Let's note that sometimes these singularities, which belong to one type of the centers, but for two different values of θ ($\theta = 90°$ и $\theta \approx 57°$), are considered as signals from the various centers.

The analysis of a spectrum **IV** (Fig. 5a1) shows that parameters of its spin Hamiltonian are equal: $g = 2.0008 \pm 0.0005$, $A = (74.1 \pm 0.3)\cdot10^{-4}$ cm^{-1} and $D = (30 \pm 10)\cdot10^{-4}$ cm^{-1}. Such signal should be carried to presence of the second phase in the samples. One of the basic products accompanying superfine powders at storage on air, are hydroxides, which form on surface of particles [27]. Unfortunately, in the literature data of spin-Hamiltonian parameters for EPR spectrum Mn^{2+} ions in $Zn(OH)_2$ lattice are absent. Crystal phases of $Zn(OH)_2$ have rhombohedral or trigonal symmetry. It is known that small values of parameters of a ground-state splitting in crystal field is typifying for Mn^{2+} ions in trigonal $Mg(OH)_2$ ($D = 7.8\cdot10^{-4}$ cm^{-1} and $a = 11\cdot10^{-4}$ cm^{-1} [28]). The $Mg(OH)_2$ is isostructural to trigonal $Zn(OH)_2$. Thus, most likely, the spectrum **IV** is caused by Mn^{2+} ions in core-shell of $Zn(OH)_2$. EPR data allow to make a rough estimation of the content of the phase. We consider that linewidth, ΔB, for the ions Mn^{2+} ($\Delta B \approx 9$ Gs for central transition) is caused by the dipole–dipole widening.

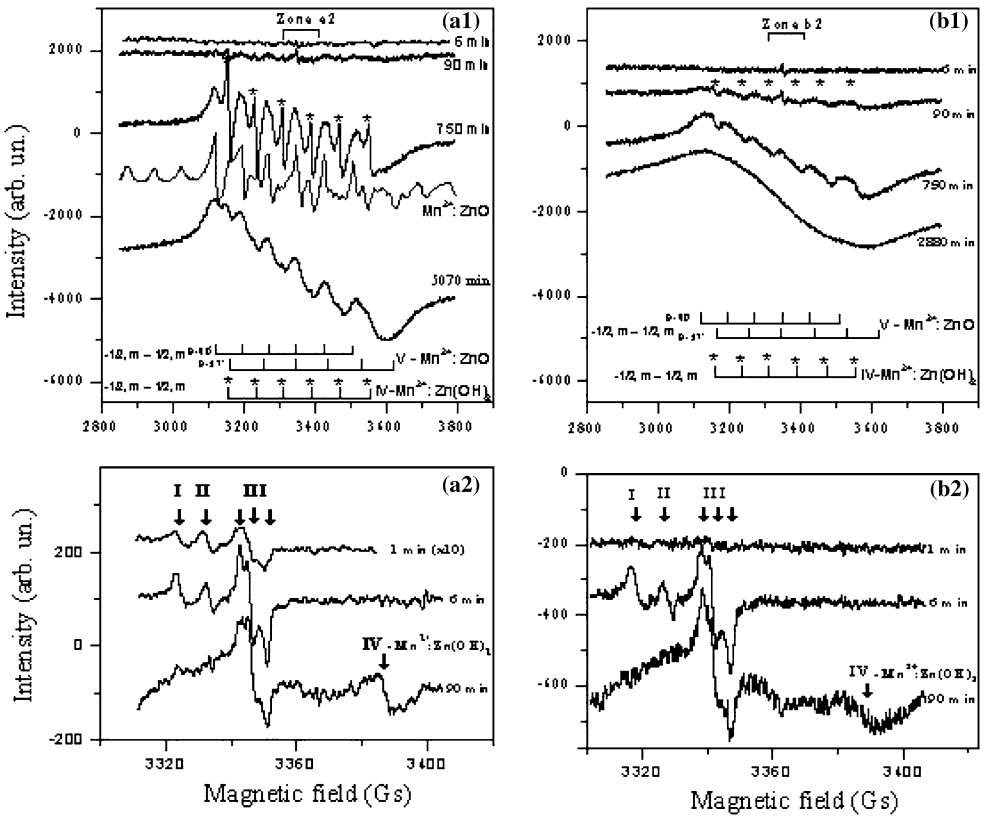

Fig. 5 EPR spectra obtained during MT for samples (***a***) (**a1**, **a2**) and (***b***) (**b1**, **b2**) samples. (**a2**) and (**b2**) show the spectra of electron-hole paramagnetic centers **I**, **II** and **III**

Between the width of a line and concentration, c, of the centers with spin S = 5/2 exists correlation

$$\Delta B = 12.0(\mu_0/4\pi)\beta g(c/d^3), \quad (5)$$

where d is shortest distance between paramagnetic ions [29]. From here follows that the concentration of Mn^{2+} ions in the second phase is ~0.1 at.%. The content of ions of Mn^{2+} (spectrum IV) in the 50 mg of sample after t_{MT} = 390 min. is N ~ $3{\cdot}10^{15}$. The estimation was made by comparison with an EPR signal from the standard sample. Thus, in the sample the content of atoms of the second phase is $N/c \sim 3{\cdot}10^{18}$. This corresponds to ~0.5% of the general content of atoms in the sample. At localization of such quantities of other phase on a surface of formed particles of ZnO (d ~ 150 nm), the thickness of the surface layer will be ~0.2 ÷ 0.4 nm. The presence of the $Zn(OH)_2$ in initial and grinded samples of ZnO (the content of which increases with an increase of t_{MT}) is confirmed by data of IR spectroscopy (see Fig. 3, the absorption band at ν ~ 3,400 cm^{-1}). Note that presence of the $ZnO/Zn(OH)_2$ core-shell structure was established in samples ZnO prepared via the wet chemical method [23].

The strict measurement of quantitative changes of a spectrum **IV** has appeared inconvenient both because of a concentration widening of HFS-lines and because of superposition with signal **V**, the intensity of which intensively was increasing. Coarse estimates show that intensity of a spectrum **IV** is little more in samples ***a*** than in ***b***.

The general character of change of an integrated intensity of spectra **I**, **II**, **III**, **IV,** and **V** for the sample ***a*** is shown on Fig. 6. The changes of spectrum **V** in samples ***a*** and ***b***, as a whole, are proportional to the content in them of additives of MnO_2.

Discussion

Let's consider results with a point of view of consecutive evolution of structure of defects in mixtures at prolonged

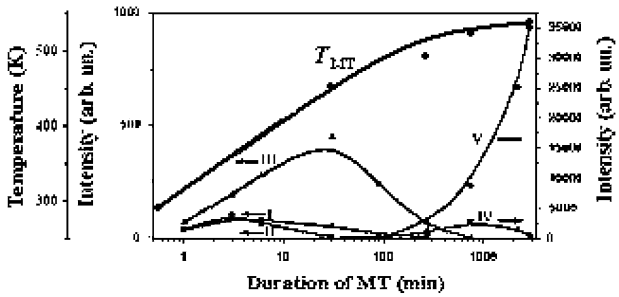

Fig. 6 The dependence of the intensity in EPR spectra (**I**, **II**, **III**, **IV**, and **V**) and the temperature of sample, T_{MT}, on the MT duration of the sample 99%ZnO + 1% MnO2

MT. Generally, as it was marked above, a process of grinding-activation represents the rolling of crushing balls on a layer of a mixture of powders ZnO + xMnO$_2$ in the bottom part of jars. At the initial moment a mill (jars and balls) and the sample are at room temperature. Let's begin from assumption that in a zone of destruction (and deformations) there is a formation of a wide set of defects (both in ZnO, and in MnO$_2$), which have various physical and chemical properties [30]. Some of formed defects can interact with atoms of an environment even at room temperature. For example, it is known that concentration of PC, formed at MT of ZnO in vacuum, decreases in 10 times at an admitting of air in jar [31]. Such changes reflect, at least, 2 moments: (a) the high reactivity of PC, which is localized on an external surface. PC in this case have worked as the centers of absorption; (b) the presence in particles of zones of defects formation, which are closed from such contacts (for example, inside of microcracks). In turn, the formation of defects is accompanied by development of various mechanothermic processes (impulsive, periodical, connected with rolling-process, and accumulative) which actively modify an initial defect structure. Thus, the set of defects and other formed states in an end-product will be defined by a set of concrete conditions: by regimes of MT, temperature condition, the environment of processing and storage, etc.

X-ray data (Figs. 1, 2) reflect the general process of accumulation of defects in samples with increase in duration MT whereas data FTIR (Figs. 3, 4) and EPR (Figs. 5, 6) allow differentiating a set of defect states.

Let's estimate the temperature of the sample developed during MT, using data in Fig. 6 and data on annealing temperature of samples. So, it was established that signal **II** disappeared after an annealing at T_{treat} ~ 453 K; signal **I** disappeared after treatment at T_{treat} ~ 493 K; and signal **III** disappeared after treatment at T_{treat} ~ 533 K. We consider that in the moment of disappearance of signals **I**, **II** and **III** ($t_{MT} = t_{dis}$) in the sample the specified above temperature are reached. It allows constructing the diagram of change of average temperature of the sample from duration of MT, $T_{MT} = f(t_{MT})$ (see Fig. 6, curve T_{MT}). Achievement of equilibrium temperature, Teq ≈ 543 K, at $t_{MT} > 750$ min reflects conditions, when the quantity of received and dissipated heat by the sample is equal.

Considering variety of existing defect states and distinction of their annealing activation energy, E_{act}, it is possible to conclude that a change of MT duration varies a set of defects in the sample (especially at initial stage MT) in a direction of accumulation of defects with greater energy activation of annealing.

Consecutive (in all range of t_{MT}) growth of intensity of OH and CO bands of absorption in samples with small concentration MnO$_2$ (sample ***a***) shows that the defect states **H** and **C** (which are responsible for processes of hydration and carbonation on surfaces of MT ZnO) have greater (than for the centers of type **I**, **II** and **III**) values of E_{act}. The analysis shows that the basic processes of hydration and carbonation of samples take place at storage in air, instead of at MT. It is caused by a low content of water vapor and oxide carbon presents in a jars.

However, distinction in behaviors of curves of accumulation of these defect states in samples ***a*** and ***b*** (Fig. 4) also indicates on participation of these defects in reaction of interaction with oxides of manganese. The centers, which have formed as a result of such reaction, do not interact any more with groups OH or CO$_2$ at storage of the samples on air. Such reaction is promoted with an increase of t_{MT} (growth T_{MT}). In samples with bigger content of MnO$_2$ (sample ***b***) comes the moment (t_{MT} ~ 20–90 min), after which the quantity of **H** and **C** centers starts to decrease (Fig. 4).

The occurrence of an EPR signal **IV** (Mn^{2+} in Zn(OH)$_2$) is observed at $t_{MT} \geq 90$ min. At that the temperature of sample is ~453 K. Then the intensity, I_{IV}, of the signal is increased. Achievement of maximal value occurs at t_{MT} = 750 min. This corresponds to T_{MT} ~ 493 K. The appearance of this signal reflects interaction of superficial defects of ZnO and MnO$_2$ with each other and with groups of OH of the gas environment and the formation of Zn(OH)$_2$. The absence in EPR spectra of signals from SDC in samples ***a*** and ***b*** also is connected with process of interaction of the superficial defects with oxides of manganese.

The observed changes of **V** spectrum depending on t_{MT} are similar to the changes of the spectrum in samples ZnO + xMn$_2$O$_3$ treated during different time at constant temperature [32]. However is necessary to note that process of mechanical doping ZnO by ions Mn^{2+} is accompanied also by the continuous increase (or keeping the certain level) of defects concentration in ZnO. Therefore the rapidity of changes of concentration I_V in case of MT should be bigger than in case of thermal treatment at $T = T_{eq}$. It can be facilitated also by the local moving of ZnO and MnO$_2$ particles in the moments of loading-unloading.

Computer simulations of EPR spectra carried out by a previously described method [25] have shown that each spectrum can be accounted for as a superimposition of two spectra (''narrow'' and ''broad'') having the same spin-Hamiltonian parameters but with different intrinsic line width. The ''broad'' and ''narrow'' spectra can be attributed, respectively, to regions near and far with regard to the diffusion sources (MnO$_2$ particles). The average content of Mn^{2+} ions on the boundary of the diffusion source (calculated from magnitude of broad signal width, ΔB ≈ 110 Gs (see (5)) for samples ***a*** and ***b*** corresponds to ~1.5%.

These data are one more confirmation of the limiting low solubility (~2–3%) of manganese atoms in a ZnO lattice. Average concentration of ions of manganese in samples is defined a dipole width of lines in a ''narrow'' spectrum (see (5)). So for samples ***a*** and ***b*** after MT during 2,880 min widths of hyper fine structure EPR-lines Mn^{2+}:ZnO were: $\Delta B_a \approx 35$ Gs and $\Delta B_a \approx 90$ Gs. It corresponds to 0.25% at. Mn^{2+} ions in sample ***a***, and is 0.8% at. in the sample ***b*** (see (5)).

Conclusions

Presented results allows to propose a general evolution scheme of defects formation and reaction process in mixtures ZnO + 1%MnO_2, and ZnO + 10%MnO_2 during prolonged MT. The initial powder and mill are at room temperature. At MT in zones of deformation-destruction different defects (V_{Zn}^{-}:Zn_i^0 (**I**), V_{Zn}^{-} (**II**), and $(V_{Zn}^{-})_2^{-}$ (**III**) centers at all) are forming. Defects have various physical and chemical properties, and different activation energies of annealing, E_{act}. Formed defects are interacting with each other and with atoms from the environment (air, additives, material of a grinder, cohesion processes). The part of these defects is responsible for the processes of hydration and carbonation of samples. In turn, the formation of defects is accompanied by development of various mechanothermical processes, which increase temperature of the sample, T_{MT}. The increasing of T_{MT} activates the reactionary processes: leads to formation $Zn(OH)_2$, doped with Mn^{2+} ions, and also promotes a consecutive annealing the «low-temperature» defects having small values of E_{act} (**I**, **II** and **III**). With an increase of $t_{MT,}$ the process of MT is accompanied by an increasing of temperature of samples up to equilibrium, and accumulation of ''high-temperature'' defects in the sample. T_{eq} is characteristic for concrete conditions of the experiment (process conditions, the set of balls, quantity of the sample, the jars and balls material and at all). As a result, in the sample the conditions for an intensification of volumetric diffusion processes, formations of Mn^{2+}-doped ZnO are created. It is possible to present that the MT of powders mixtures can be an interesting technological method of production of doped particles of different materials.

References

1. Gupta TK (1990) J Am Cer Soc 75:1817
2. Furdyna JK (1988) . Diluted magnetic semiconductors. Academic, New York
3. Bates CH, White WB, Roy R (1966) J Inorg Nucl Chem 28:397
4. Mizokawa T, Nambu T, Fujimori A, Fukumura T, Kawasaki M (2002) Phys Rev B 65:085209
5. Fukumura T, Jin Z, Ohtomo A, Koinuma H, Kawasaki M (1999) Appl Phys Lett 75:3366
6. Jin Z, Fukumura T, Kawasaki M, Ando K, Saito H, Sekiguchi T, Yoo YZ, Murakami M, Matsumoto Y, Hasegawa T, Koinuma H (2002) Appl Phys Lett 78:3824
7. Jung SW, An S-J, Yi G-C, Jung CU, Lee S-I, Cho S (2002) Appl Phys Lett 80:4561
8. Jin Z-W, Yoo Y-Z, Sekiguchi T, Chikyow T, Ofuchi H, Fujioka H, Oshima M, Koinuma H (2003) Appl Phys Lett 83:39
9. Kim YM, Yoon M, Park I-W, Lyou JH (2004) Sol St Comm 129:175
10. Norberg NS, Kittilstved KR, Amonette JE, Kukkadapu RK, Schwartz DA, Gamelin DR (2004) J Am Cer Soc 126:9387
11. Minami T, Sato H, Nanto H, Takata S (1985) Jpn J Appl Phys 24:L781
12. Zhou H, Hofmann DM, Hofstaetter A, Meyer B (2003) J Appl Phys 94:1965
13. Han S-J, Jang T-H, Kim YB, Park B-G, Park J-H, Jeong YH (2003) Appl Phys Lett 83:920
14. Kolesnik S, Dabrowski B, Mais J (2004) J Appl Phys 95:2582
15. Kolesnik S, Dabrowski B (2004) J Appl Phys 96:5379
16. Driessens FCM, Rieck GD (1966) J Inorg Nucl Chem 28:1593
17. Klug HP, Alexander LE (1974) . X-ray diffraction procedures for polycrystalline and amorphous materials, 2nd edn. J Wiley & Sons, New York
18. Liu Y, Ren W, Zhang LY, Yao X (1999) Thin Solid Films 353:124
19. Kakazey MG, Sreckovic TV, Ristic MM (1997) J Mater Sci 32:4619, DOI 10.1023/A:1018689721667
20. Kakazey MG, Vlasova M, Dominguez-Patiño M, Dominguez-Patiño G, Gonzalez-Rodriguez G, Salazar-Hernandez B (2002) J Appl Phys 92:5566
21. Schallenberger B, Hausmann A (1976) Z Physik B23:177
22. Galland D, Herve A (1974) Solid State Comm 14:953
23. Zhou H, Alves H, Hofmann DM, Kriegseis W, Meyer BK, Kachmarchyk G, Hoffmann A (2003) J Appl Phys 94:1965
24. Hausmann A, Huppertz H (1968) J Phys Chem Sol 29:1369
25. Kliava J (1988) EPR spectroscopy of disordered solids. Zinatne, Riga
26. Vlasova MV, Kakazey NG, Kostic P, Milosevic O, Uskokovic D (1985) J Mater Sci 20:1660, DOI 10.1007/BF00555269
27. Nakagawa M, Mitsudo H (1986) Surf Sci 175:157
28. Piechonka WA, Petsch HE, Mclay AB (1961) Canad J Phys 39:145
29. Berger R, Kliava J, Yahiaoui E-M, Bissey J-C, Zinsou PK, Beziade P (1995) J Non-Cryst Sol 180:151
30. Heinike G (1984) Ttribochemistry. Akademie-Verlag, Berlin
31. Politov AA, Zakrevsky VA, Izvestia SO (1988) AN SSSR 5:43
32. Kakazey M, Vlasova M, Dominguez-Patiño M, Kliava J, Tomila T (2006) J Am Cer Soc 89:1458